Uniaxial ferromagnetism of local uranium moments in hexagonal UBeGe

Roman Gumeniuk,[1,2,*] Alexander N. Yaresko,[3] Walter Schnelle,[2] Michael Nicklas,[2] Kristina O. Kvashnina,[4,5] Christoph Hennig,[4,5] Yuri Grin,[2] and Andreas Leithe-Jasper[2]

[1]*Institut für Experimentelle Physik, TU Bergakademie Freiberg, Leipziger Straße 23, 09596 Freiberg, Germany*
[2]*Max-Planck-Institut für Chemische Physik fester Stoffe, Nöthnitzer Straße 40, 01187 Dresden, Germany*
[3]*Max-Planck-Institute for Solid State Research, Heisenbergstraße 1, 70569 Stuttgart, Germany*
[4]*European Synchrotron Radiation Facility, 71, Avenue des Martyrs, Cedex 9, 38043 Grenoble, France*
[5]*Helmholtz-Zentrum Dresden-Rossendorf (HZDR), Institute of Resource Ecology, P.O. Box 510119, 01314 Dresden, Germany*

(Received 1 November 2017; revised manuscript received 24 January 2018; published 7 May 2018)

The new intermetallic uranium beryllium germanide UBeGe and its thorium analogon ThBeGe crystallize with the hexagonal ZrBeSi type of structure. Studies of magnetic, thermal, and transport properties were performed on polycrystalline samples between 1.8 and 750K. UBeGe is a uniaxial ferromagnet and there are indications for two magnetic transitions at $T_C^{(1)} \approx 160$K and $T_C^{(2)} \approx 150$K. The high paramagnetic effective moment $\mu_{\text{eff}} \approx 3.1\,\mu_B$, x-ray absorption near-edge spectroscopy (XANES, 17–300 K), as well as theoretical DFT calculations indicate localized U $5f^2$ states in UBeGe. ThBeGe is a diamagnetic metallic material with low density of states at the Fermi level.

DOI: 10.1103/PhysRevB.97.174405

I. INTRODUCTION

Being much less localized than $4f$ states, the $5f$ electrons of light actinides often exhibit a dual behavior, localized as well as itinerant [1,2], giving rise to exciting physical phenomena. One of such observations is the high sensitivity of the nature of $5f$ states to pressure, magnetic field, and alloying with other elements. These factors affect the degree of $5f$ localization, giving rise to such phenomena as magnetism, heavy fermions, superconductivity, etc. One of the characteristic features of actinide magnetism is the strong spin-orbit coupling resulting in the significant orbital polarization of the $5f$ band and, thus, leading to a huge magnetocrystalline anisotropy in uranium intermetallic compounds [3].

The magnetic behavior of U moments varies in a broad range from a weak Pauli-paramagnetic state (as, e.g., in UTB_4 (T = Ru, Os) [4,5]), to Curie-Weiss behavior with large effective magnetic moments (e.g., UFe_2Al_{10} [6]) and various magnetic orderings (ferro, antiferro, ferri, etc.) including complex magnetic structures [3]. Since the surprising discovery of ferromagnetism in UH_3 by Trzebiatowski in the early 1950s [7,8], the high-T_C ferromagnets containing uranium have been the objects of numerous investigations (see, e.g., Refs. [9,10] and references therein). The influence of different types of ligands on the U $5f$ electron states have been intensively studied. Such series of compounds are, for instance, cubic U_3X_4 (X = P, As, Sb, Bi) with T_C of 116–200 K [11,12] and its "filled-up" variants $U_3T_3Sb_4$ (X = Co, Ni, Cu) with T_C = 10–88 K [13] as well as the group of 24 UTX compounds (T = transition metal; X = p element) with hexagonal ZrNiAl-type structure. Prototypical uniaxial ferromagnets with T_C of 62 and 68 K are UIrAl [14] and UPtGa [15]. In these cases, the magnetism is thought to be predominantly due to localized U $5f$ electrons.

The two U-containing hexagonal binary compounds U_3Ge_5 [16,17] and UGa_2 [18] also show high T_C of 94 and 125 K, respectively. Recently, high-pressure electrical resistivity measurements could shed light on the magnetism of UGa_2: The change of the Curie temperature with compression of the lattice indicates here a complex influence of pressure-dependent hybridization effects on the initially rather localized state of the $5f$ electrons [18].

Among the U-containing binaries, the system U-Ge is of special interest [17,19]. There, orthorhombic UGe_2 and ternary substitution variants have been in focus of numerous investigations (see, e.g., Refs. [20–22] and references therein) due to the dual nature of U $5f$ states [23]. Being simultaneously localized and itinerant, the $5f$ electrons in UGe_2 give rise to superconductivity (T_c = 0.8 K at a pressure of 1.2 GPa) with an adjoined ferromagnetic (FM) phase (T_C = 52 K) [24–26]. The unusual phase diagram with FM and superconducting phases next to each other triggered a discussion about an unconventional superconducting state in this simple compound. One of the possible order parameters of superconductivity would be a nonunitary triplet state proposed within a phenomenological theory of FM superconductivity [27]. However, the problem of the coexistence of superconducting and FM phases has not been solved.

In order to obtain further insight, we tried to substitute Ge in UGe_2 by smaller atoms. Such approaches worked for the solid solutions YGe_2-UGe_2-USn_2 [28], UGe_2-USn_2 [22], and UGe_2-UNi_2 [29]. However, using beryllium, instead of obtaining the solid solution UBe_xGe_{2-x}, the new ternary compound UBeGe crystallizing with ZrBeSi type of structure [30] was found. Our studies of physical properties revealed UBeGe to be a strongly anisotropic ferromagnet with a large magnetization (M = 2.89 μ_B) and high Curie

*Roman.Gumeniuk@physik.tu-freiberg.de

 ©2018 American Physical Society

temperature $T_C = T_C^{(1)} \approx 160$ K, indicating a well localized nature of the U $5f$ electrons, as is the case for many UTX compounds [3].

II. SAMPLE PREPARATION AND METHODS

Samples with nominal compositions ThBeGe and UBeGe were prepared from Th (Goodfellow, 99.5 wt.% metal base, 2 wt.% of ThO_2), U (Goodfellow, 99.98 wt.%), Be (Heraeus, 99.9 wt.%), and Ge (Chempur 99.9999 wt.%). The metal pieces were arc melted (mass loss <0.5 %), placed in ZrO_2 crucibles, and sealed in tantalum tubes. The heat treatment was performed at 900 °C for 240 h. All sample handling was performed in argon-filled glove boxes [$p(O_2/H_2O) < 1$ ppm] in a laboratory with high safety standards [31].

The synthesized samples were characterized by powder x-ray diffraction (PXRD) [HUBER G670 imaging plate Guinier camera with Cu$K_{\alpha 1}$ radiation ($\lambda = 1.540598$ Å)]. High-resolution (HR) PXRD data for structure refinement were collected at the BM20-Rossendorf beamline of the European Synchrotron Radiation Facility (ESRF) ($\lambda = 0.45932$ Å, $2\theta_{max} = 40°$) on powder enclosed in a quartz capillary (outer diameter 0.5 mm). The signal was measured by eight scintillation detectors, each preceded by a Si (111) analyzer crystal. The sample was cooled down to 100 K in a N_2-flow cryostat. Phase identification was performed with the WINXPOW program package [32]. The unit cell parameters refinement by least-squares fitting as well as the crystal structure refinement was performed using the WINCSD software [33].

The temperature-dependent x-ray absorption near edge structure (XANES) spectra were measured at beamline ID26 of the ESRF [34]. The ⟨111⟩ reflection from a double Si crystal monochromator was used to select the incident energy. An x-ray emission spectrometer [35,36] was utilized to obtain XANES spectra in high-energy-resolution fluorescence detection (HERFD) mode. The intensity of the U M_β emission line (3336.0 eV) measured as function of the incident energy provided U HERFD spectra at the M_4 edge. The emission energy was selected using the ⟨220⟩ reflection of five spherically bent Si crystal analyzers (with 1 m bending radius) aligned at Bragg angle of 75°. The paths of the incident and emitted x rays through air were minimized in order to avoid losses in intensity due to absorption. A combined (incident convoluted with emitted) energy resolution of 0.7 eV was obtained by measuring the full width at half maximum (FWHM) of the elastic peak.

The magnetization was determined in MPMS-XL7 and MPMS3 magnetometers (Quantum Design). Measurements were performed on both a polycrystalline bulk piece and on a specially prepared powder sample. For the latter, a calibrated quartz tube was filled with 12.4 mg UBeGe powder, 61.6 mg germanium powder, and 2-methylpentane (C_6H_{14}, melting point 113–127 K). The sealed tube allows cooling the powder suspended in liquid to temperatures below the magnetic ordering of UBeGe. In order to align the magnetic crystallites of UBeGe, the mixture was allowed to freeze with applied magnetic fields. Electrical resistivity and heat capacity were measured in a commercial system PPMS9 with ACT or HC option, (Quantum Design) and using an ac resistance bridge (LR-700, Linear Research). Electrical contacts were made with silver-filled epoxy (EPO-TEK H20E).

Band structure calculations were performed for the experimental crystal structure of UBeGe using the linear muffin-tin orbital (LMTO) method [37] as implemented in spin-polarized relativistic PY LMTO computer code [38]. The Perdew-Wang parametrization [39] was used for the exchange correlation potential in the local spin density approximation (LSDA). XANES spectra were calculated based on LSDA in the dipole approximation, neglecting the effect of a core hole. In order to understand better details of U $5f$ hybridization with Be- and Ge-derived bands, we also performed calculations for ThBeGe using its experimental crystal structure data.

III. RESULTS AND DISCUSSION

A. Crystal structure

All peaks in the PXRD patterns of UBeGe and ThBeGe were indexed in the hexagonal lattice with unit cell parameters given in Table I. The analysis of the systematical absences indicated possible space groups $P6_3mc$, $P\bar{6}2c$, or $P6_3/mmc$. Therefore, the simple structural model of the ZrBeSi-type [30] was chosen for the Rietveld refinement. The observed, theoretically calculated, and differential profiles for UBeGe, which correspond to the low reliability factors, are presented in Fig. 1. The crystallographic details of the refinements for UBeGe and ThBeGe are collected in Table I.

To detect possible structural phase transitions of UBeGe we performed HR-PXRD measurements above and well below the magnetic ordering temperature at ≈160 K. No such changes were noticed between 100 and 298 K (see Table I). The full width at the half maxima of all reflections varies in the narrow range of 0.03-0.04° (Fig. 1), which is typical fof HR-PXRD patterns and indicates no split, atypical asymmetry or broadening of the peaks. Thus, the ZrBeSi-type structure persists also below the magnetic transition temperature.

TABLE I. Crystallographic data for UBeGe and ThBeGe: structure type ZrBeSi, space group $P6_3/mmc$, $Z = 2$, [Ac = U or Th in $2a$ (0 0 0); Be in $2c$ (1/3 2/3 1/4); Ge in $2d$ (1/3 2/3 3/4)].

Compound	UBeGe	UBeGe	ThBeGe
Temperature (K)	100	293	293
a (Å)	3.8862(3)	3.8947(2)	3.9658(4)
c (Å)	8.1364(6)	8.1536(5)	8.5340(8)
V (Å^3)	106.42(2)	107.11(3)	116.24(3)
ρ (g cm^{-3})	9.97(1)	10.00(1)	8.96(1)
Diffraction setup	BM20A	G670	G670
Wavelength (Å)	0.45932	1.540598	1.540598
B_{iso} (Å^2), Ac	1.0(2)	0.9(1)	0.8(1)
B_{iso} (Å^2), Ge[a]	1.4(4)	1.0(3)	0.9(3)
R_I, R_P (%)	4.2, 8.9	3.8, 7.6	4.8, 8.6
$d_{(Ac-6Ac)}$ (Å)	3.8862(2)	3.8946(2)	3.9657(3)
$d_{(Ac-6Ge)}$ (Å)	3.0285(1)	3.0350(1)	3.1296(2)
$d_{(Be-3Ge)}$ (Å)	2.2437(1)	2.2486(1)	2.2896(2)

[a] B_{iso} for the Be atoms was fixed to 1.0 Å^2.

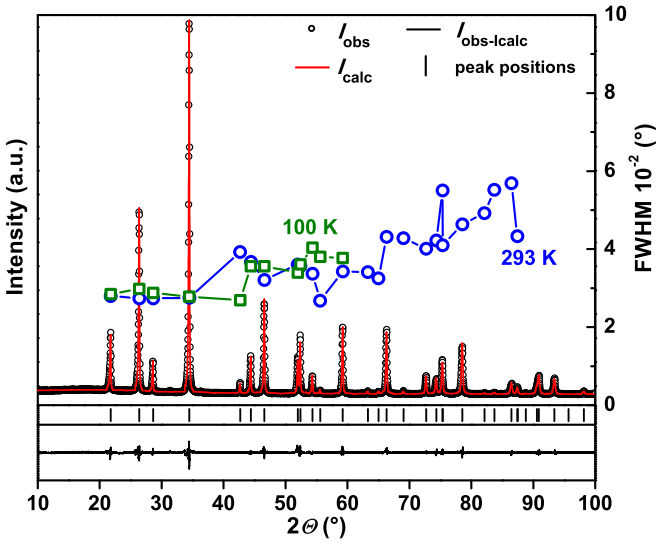

FIG. 1. Powder x-ray diffraction pattern of UBeGe together with the full width at half-maxima (FWHM) of the reflections (blue, green, right scale) observed in the HR-PXRD data sets.

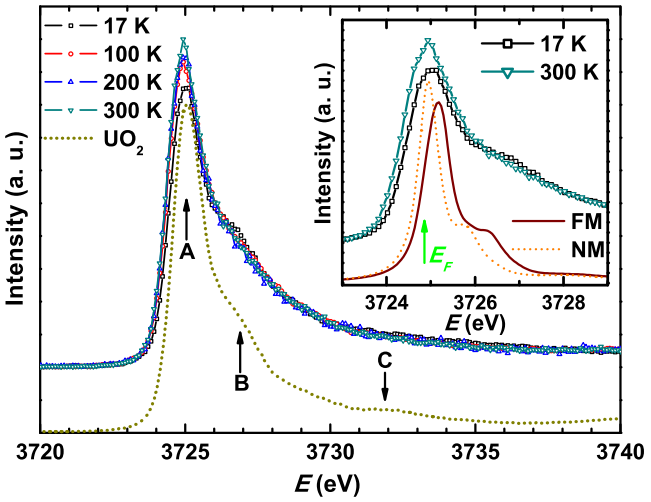

FIG. 3. HERFD XANES spectra at the uranium M_4 edge for UBeGe and UO_2. Inset: theoretically calculated U M_4 XAS of UBeGe assuming FM and NM structures in comparison with experimentally obtained spectra. The green arrow indicates the Fermi level E_F.

The relationship between AlB_2 and ZrBeSi structure types was widely discussed in the literature [40,41]. For a better visualization, we depict in Fig. 2 crystal structures of $UGe_{1.57}$ crystallizing with the AlB_2 type [16] and UBeGe (ZrBeSi-type). Both of them can be understood as alternating nets along [001] direction. The hexagonal net consisting in both structures solely of U atoms, alternate with ones built up of exclusively Ge atoms ($UGe_{1.57}$) or contains equal amounts of Ge and Be atoms (UBeGe). The Ge or Be atoms reside in both structures in the trigonal prisms formed by U. All these lead also to the change of lattice parameter c: It is doubled in all compounds crystallizing with ZrBeSi type compared to the AlB_2 type.

The interatomic distances in the structures of UBeGe and ThBeGe (Table I) agree mostly well with the sums of atomic radii of the elements [42]. A shortening by 3–5% is only observed for Ge-Be contacts. The U-U distances are well above the Hill limit, estimated as $d_{(U-U)} = 3.5$ Å [43]. This should indicate a localized nature of the U 5f electrons in the structure of UBeGe.

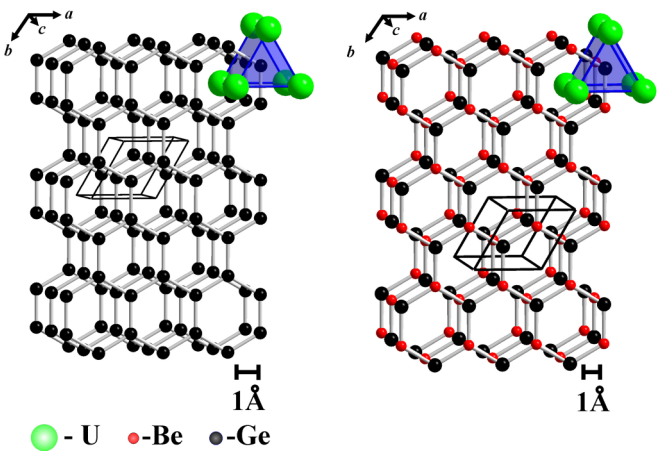

FIG. 2. Condensed $[Ge_6]$ and $[Ge_3Be_3]$ hexagonal rings together with $[GeU_6]$ trigonal prisms in the structures of $UGe_{1.57}$ and UBeGe.

B. XANES

To directly probe the valence state of uranium atoms (i.e., U 5f shell) [44] in UBeGe, we performed XANES (HERFD) measurements at the U M_4 edge at different temperatures. The HERFD spectra of the intermetallic compound UBeGe and of the oxide UO_2 are shown in Fig. 3. The strongest white lines (features A and B) occur almost at the same energy for both compounds and the only difference is that for UBeGe they are slightly broader. The pronounced feature C in the spectrum of UO_2, as well as other high-energy white lines (visible in Fig. 4 of Ref. [45]) appearing in the oxide due to the U-O bonding, are not observed for UBeGe. This indicates that surface contamination with an oxide is unlikely.

Since the main features A and B in the HERFD spectra of UBeGe and UO_2 are observed almost at the same energies and they have close values of FWHM, one can assume an oxidation state +4 (i.e., the $5f^2$ configuration) for the U atoms in UBeGe. Interestingly, in contrast to $U_3Ir_4Ge_{13}$ [45] and UPd_3 [46], where an energy shift of the main spectral features in comparison to UO_2 is observed, the spectrum of UBeGe almost coincides with the one of the oxide. This indicates much weaker screening of the core hole by conduction electrons [47] in UBeGe than in the mentioned intermetallic compounds.

The intensity of feature A increases with temperature (Fig. 3), while feature B becomes weaker. Such a behavior of white lines in XANES of systems containing 4f elements indicates a temperature-dependent intermediate-valence state of rare-earth atoms [48]. For an U-containing intermetallic compound it is observed for the first time. To understand this phenomenon, we performed DFT calculations assuming ferromagnetic (FM) and nonmagnetic (NM) structures for UBeGe. The contribution of U 5f electrons to the electronic

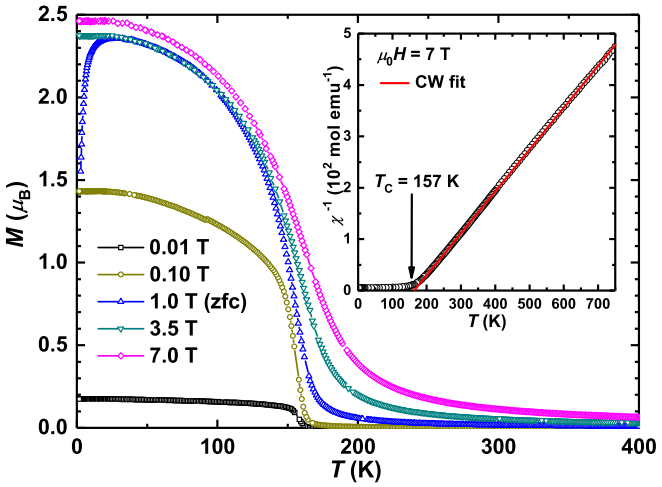

FIG. 4. Temperature dependence of the magnetization $M(T)$ of UBeGe (bulk sample, field cooling). Inset: inverse magnetic susceptibility H/M in a field $\mu_0 H = 7$ T; the line shows a fit to the Curie-Weiss (CW) law for $T > 300$ K.

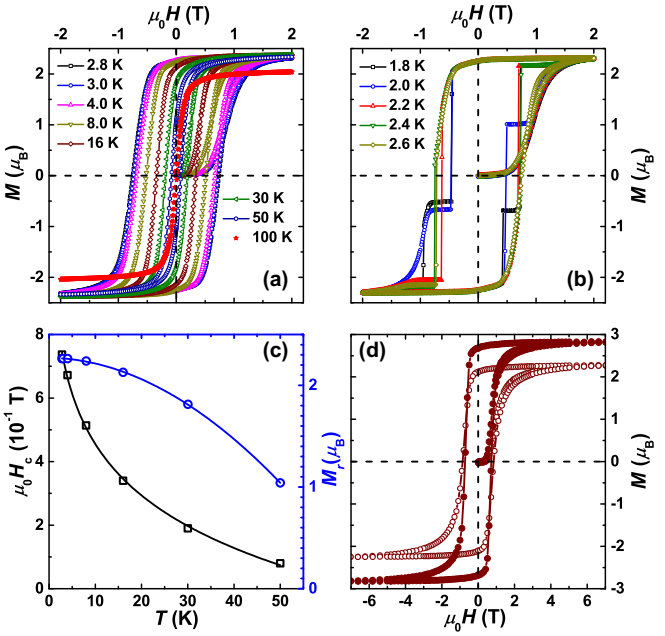

FIG. 5. (a) Isothermal magnetization curves $M(H)$ of UBeGe (bulk sample, after zero-field cooling from 200 K). (b) Magnetic hysteresis at low T showing stairlike behavior for $T \leqslant 2.6$ K. (c) Temperature dependencies of coercive field $\mu_0 H_c$ (left scale) and remanence M_r (right scale). (d) Isothermal magnetization curves $M(H)$ at $T = 2$ K for UBeGe powder aligned during field-cooling (•) and cooled in zero field (○).

density of states (DOS; shifted to coincide with feature A) are shown in Fig. 3 inset. The calculated U $5f$ DOS is narrower than the experimentally measured spectrum, but nevertheless nicely reproduces both main spectral features A and B. Also, the U $5f$ DOS of the FM structure shows weaker intensity for feature A and is slightly shifted toward higher energies in comparison to the NM structure. Temperature decrease (i.e., transition from NM to FM states) causes also the decrease of the intensity of feature A and its slight shift toward higher energy. Both effects are clearly seen in the HERFD spectra of UBeGe at 300 and 17 K (Fig. 3 inset). Therefore, we conclude that the variation of the intensities of the spectral features of UBeGe with temperature is of magnetic origin.

C. Magnetic properties

The thorium compound ThBeGe is a diamagnet. Magnetic susceptibility data $\chi(T)$ measured in various fields demonstrate the absence of para- or ferromagnetic impurities. Remarkably, $\chi(T)$ varies almost linearly between $-120(10) \times 10^{-6}$ emu mol^{-1} at $T = 400$ K and $\chi_0 \approx -85(10) \times 10^{-6}$ emu mol^{-1} at $T \to 0$. No anomalies or superconductivity were observed down to 1.8 K.

The temperature dependence of the magnetization M of bulk UBeGe in different applied fields is presented in Fig. 4. $M(T)$ measured in a field $\mu_0 H = 10$ mT shows a sharp FM transition at $T_C = 157$ K. Larger applied fields shift the anomaly to higher T and lead to an increase of the magnetization. For this polycrystalline sample, a maximum magnetization of $M = 2.46\ \mu_B$ is observed at $T = 1.8$ K and $\mu_0 H = 7$ T. Measurements performed in warming after zero-field cooling (only one curve shown for $\mu_0 H = 1.0$ T) revealed the typical drastic increase at a temperature depending on the applied field, indicating strong magnetocrystalline anisotropy [49–51].

For temperatures well above the FM transition (300–750 K), the magnetic susceptibility of UBeGe fits excellently a Curie-Weiss type law (Fig. 4 inset) with effective magnetic moment $\mu_{eff} = 3.14\ \mu_B$ and paramagnetic Curie temperature $\theta_P = 163$K. The obtained μ_{eff} is close to those reported for the c direction in UGe_2 ($\mu^c_{eff} = 3.02\ \mu_B$) [52], for the b direction in UPtGe ($\mu^b_{eff} = 3.24\ \mu_B$) [51] and for the a direction in UIrGe ($\mu^a_{eff} = 3.40\ \mu_B$) [50] (for UBeGe we also expect an anisotropy of the effective magnetic moments). The U atoms in all above-mentioned germanides are reported to possess a $5f^2$ configuration. Thus, also the magnetic susceptibility data of UBeGe are compatible with this electronic state, in agreement with our XANES and theoretical DFT studies.

Isothermal magnetization loops of UBeGe at selected temperatures [Figs. 5(a) and 5(b)] show pronounced hysteresis and evidence the FM order. However, a strong rise of initial $M(H)$ at low fields, as expected for typical ferromagnets, occurs only for relatively high temperatures. For lower T, the magnetization remains small up to fields close to the coercive field and only then rises strongly. Such a behavior is typically connected to a strong pinning of the domain walls, in agreement with the discussion above on the $M(T)$ curve recorded in warming after zero field cooling (ZFC) (Fig. 4).

Additionally, at very low temperatures the $M(H)$ curves show an exotic stairlike behavior [Fig. 5(b)]. The phenomenon is most pronounced at 1.8 K and is completely gone at 2.8 K. Huge jumps occur suddenly in the demagnetization curves, and the field strength H_{jump} where the first jump occurs decreases with decreasing T. H_{jump} is much less than the coercive field at 2.8 K [cf. Fig. 5(c)]. The same phenomenon has been observed for UGe_2 [53–56]. Such steps (or series of steps forming a stair) have been discussed to be due to resonant quantum tunneling, random field, or intrinsic pinning of magnetic domain walls [57]. The first scenario foresees the

fields for the jumps to be temperature independent [58], which is not the case for UBeGe. The reproducibility of the steps in the different measurement runs (same cooling, same field-sweep rate) excludes the presence of random fields.

Because of the lack of single crystals, in order to obtain the saturation magnetization along the assumed easy axis in UBeGe and to eventually shed some light on the origin of the steplike behavior, the magnetization of a specially prepared powder sample (for details see Sec. II) was measured. The measured magnetization of oriented UBeGe powder [Fig. 5(d)] is significantly larger than for the polycrystalline bulk piece [Fig. 5(a)]: In the field $\mu_0 H = 7$ T, a saturation magnetization $M_{\rm sat} = 2.89\,\mu_{\rm B}$ is attained. Such a value indicates a well localized nature of the U $5f^2$ state. The success of this orientation experiment confirms also the assumed uniaxial magnetic structure. Conversely, freezing of the suspension in zero field results in a magnetization ($M_{\rm sat} = 2.27\,\mu_{\rm B}$ at 2.0 K and 7 T) slightly lower than for the bulk sample.

No steps are seen in isothermal $M(H)$ curves for the powder samples. We therefore speculate that the stairlike behavior in bulk UBeGe is due to avalanches of domain wall motions (Barkhausen noise) which is present for all strongly anisotropic ferromagnets. Besides in UGe_2, such phenomenon have been observed at $T \ll T_{\rm C}$ in Nd-Fe-B and Sm_2Co_{17} sintered magnetic material [59–61]. Measurements on single crystals, under different cooling conditions, with variation of the field-sweep rate, and down to lower T are desirable for the clarification of the mechanism of this phenomenon.

The highest coercive field strength observed is $\mu_0 H_{\rm c} = 0.74$ T at 2.8 K [Fig. 5(c); a similar value is measured for the powder sample]. Because of the alignment of the crystallites, the remanence at 2.0 K is higher for the powder sample ($M_{\rm r} = 2.67\,\mu_{\rm B}$) than for bulk UBeGe. Both these magnetic characteristics expectedly decrease with increasing T and $M_{\rm r}$ becomes very small for $T \geqslant 100$ K. To establish the magnetic structure of UBeGe, small single crystals for magnetization measurements as well as neutron diffraction data on a large powder sample are desirable.

D. Electrical resistivity

The electrical resistivity $\rho(T)$ of ThBeGe (Fig. 6) increases smoothly with increasing temperature in the range 1.8–320 K. The polycrystalline material has high residual and room-temperature resistivity (170 $\mu\Omega$ cm). $\rho(T)$ of ThBeGe fits excellently to the Bloch-Grüneisen (BG) formula

$$\rho(T) = \rho_0 + A\left(\frac{T}{\Theta_{\rm R}}\right)^n \int_0^{\Theta_{\rm R}/T} \frac{x^n}{(e^x-1)(1-e^{-x})}dx \quad (1)$$

with the residual resistivity $\rho_0 = 88.9(3)\,\mu\Omega$ cm (defect scattering), $A = 7.04(1)\,\mu\Omega$ cm depending on the phonon contribution, the Debye temperature $\Theta_{\rm R} = 492(2)$ K, and $n = 2$, which implies that scattering is dominated by electron-electron interactions [62]. $\Theta_{\rm R}$ deduced from the BG fit is larger than $\Theta_{\rm D}$ obtained from specific heat (see below) since in the BG approach only longitudinal phonon modes are included [63].

The resistivity of UBeGe decreases linearly from 170 to 320 K and fits well to $\rho_0 + BT$ with $\rho_0 = 1.65(1)$ mΩ cm and $B = -0.26(1)\,\mu\Omega\,{\rm cm\,K^{-1}}$ (Fig. 6). Linear behavior with a larger slope ($\rho_0 = 1.58(1)$ mΩ cm, $B = -0.57(1)\,\mu\Omega\,{\rm cm\,K^{-1}}$) is also observed for the U $5f$ resistivity, obtained after subtraction of the phonon contribution of ThBeGe. For ferromagnets such as UGe_2 [23] and UCu_2Si_2 [64], a logarithmic decrease of $\rho(T)$ above $T_{\rm C}$ is reported. The coexistence of ferromagnetism and Kondo effect in these compounds was explained with the so-called underscreening Kondo-lattice theory [2]. Such a scenario cannot be excluded for UBeGe.

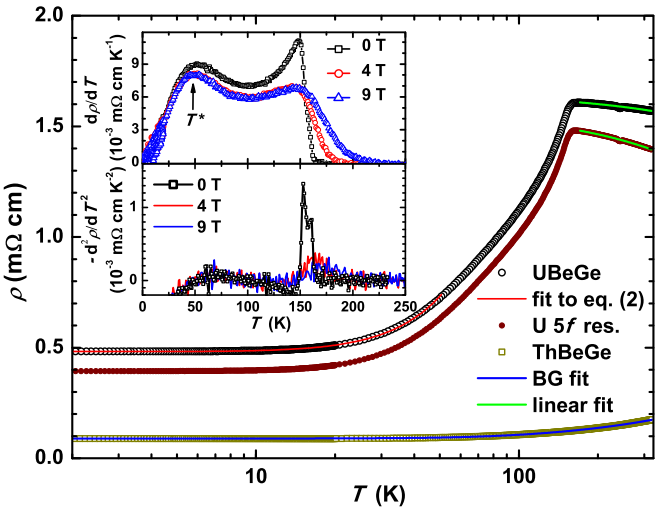

FIG. 6. Electrical resistivity ρ vs T for ThBeGe and UBeGe together with the BG fit [Eq. (1)] for 1.8–320 K and Eq. (2) for 1.8–40 K, respectively. The high-temperature resistivity (180–320 K) of UBeGe and the U $5f$ contribution are described by linear fits with negative slope. Inset: first and second derivatives around the transitions for different magnetic fields.

For UBeGe, a pronounced change is visible in $\rho(T)$ at 152 K. Below this temperature, $\rho(T)$ passes through a broad anomaly centered at $T^* \approx 50$ K and then drops to its lowest value $\rho_0 = 0.482(7)$ mΩ cm. Both temperatures can be well determined from the derivative of $\rho(T)$ (Fig. 6, upper inset) as a peak and a hump, respectively. The anomaly at T^* is independent from field and similar humps are reported for UGe_2 [23] and UCu_2Si_2 [64] single crystals. In both cases, the hump is direction dependent. For UGe_2 it is explained with the possible formation of a spin density wave [52]. Instead, we assume that it is due to the complex magnetic ordering of UBeGe (cf. Sec. III E). The second derivative of $\rho(T)$ for UBeGe suggests a splitting of the magnetic ordering anomaly ($T_{\rm C}^{(1)} \approx 161$ K and $T_{\rm C}^{(2)} \approx 153$ K; see Fig. 6, lower inset), which could be an indication for a complex magnetic ordering.

In anisotropic ferromagnets, the excitation of spin waves with energy gap Δ in the spectrum is an additional source of scattering for conduction electrons. In the electrical resistivity, this contribution is reflected by

$$A_i T^2 e^{-\Delta/T}. \quad (2)$$

With a constant background of $\rho_0 = 0.482(7)$ mΩ cm, $A_i = 0.123(9)\,\mu\Omega$ cm, and $\Delta = 10.7(3)$ K, the data of UBeGe in the range 1.8–40 K fit well to this excitation (Fig. 6). The obtained Δ is of the same order of magnitude as those reported for U-containing ferromagnets such as UCu_2Si_2 ($\Delta = 40$ K) [64] and U_2Fe_3Ge [65].

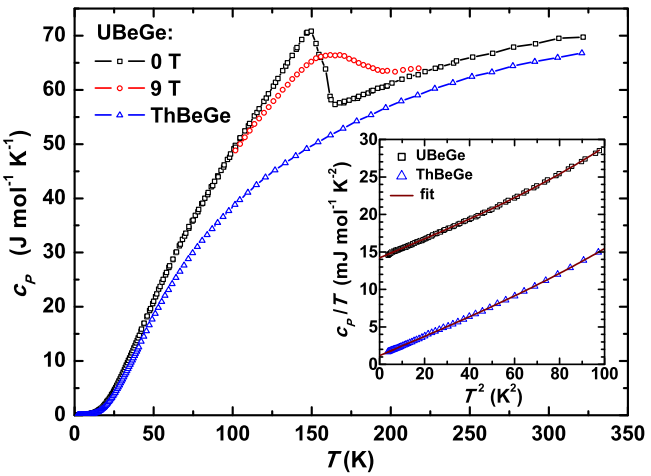

FIG. 7. Specific heat c_p as a function of temperature T in different magnetic fields for UBeGe and ThBeGe. Inset: low-temperature specific heat for UBeGe and ThBeGe in c_P/T vs T^2 presentation together with fit (see text).

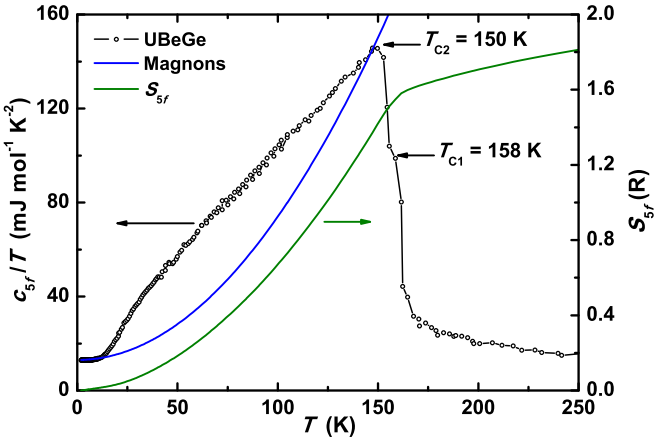

FIG. 8. The $5f$-derived specific heat contribution c_{5f}/T of UBeGe (black) after subtraction of c_p/T of ThBeGe and the simulated magnon contribution (blue line, see text). The magnetic $5f$ entropy for UBeGe is given by the green line.

The magnetoresistance (MR) of UBeGe is positive at low T (+6.5 % at $\mu_0 H = 9$ T), decreases linearly with increasing T, becomes negative at 63 K, and then shows a negative peak (−10 %) at $T_C^{(2)}$. While the positive MR at low T is also observed for a UGe_2 single crystal [64], the magnitude of MR is smaller for polycrystalline UBeGe. Interestingly, the negative MR in UBeGe vanishes only gradually above T_C and is visible to ∼250 K.

E. Specific heat

The specific heat $c_p(T)$ of UBeGe and of the reference compound ThBeGe is shown in Fig. 7. A sizable λ-like anomaly with onset at $T_C = 155$ K corroborates the long-range nature of the magnetic ordering in UBeGe. This anomaly shifts toward higher temperatures and broadens in magnetic field (data shown for $\mu_0 H = 9\,T$), which is a typical behavior for ferromagnets. In the temperature range 1.8–10 K, the specific heat of both UBeGe and ThBeGe is fitted excellently by $\gamma T + \beta T^3 + \delta T^5$ (Fig. 7 inset). The parameters of the fit are the Sommerfeld coefficient of the electronic specific heat $\gamma =$ 14.38(5) [1.31(3)] mJ mol^{-1} K^{-2}, $\beta = 0.110(5)$ [0.115(6)] mJ mol^{-1} K^{-4} (indicating a Debye temperature $\Theta_D = 375$ [370] K) and $\delta = 3.5(7)$ [2.5(1)] $\times 10^{-4}$ mJ mol^{-1} K^{-6} for UBeGe [ThBeGe]. The Sommerfeld coefficients γ indicate a density of states (DOS) at E_F of ≈6.1 and ≈0.5 states eV^{-1} f.u.$^{-1}$ for UBeGe and ThBeGe, respectively. The low γ of ThBeGe is in good agreement with the value calculated from the band structure (see Sec. III F).

In order to analyze the magnetic, $5f$-electron-derived contributions to $c_p(T)$ of UBeGe (c_{5f}), the specific heat of ThBeGe (s plus p electron and phonon contributions only) is subtracted. Plotting these as c_{5f}/T in Fig. 8, a shoulder becomes visible in the falling flank of the anomaly, suggesting two transitions at $T_C^{(1)} = 158$ K and $T_C^{(2)} = 150$ K. This would be in line with our resistivity data (Fig. 6, lower inset). The presence of two anomalies seen in $d\rho/dT$ and c_{5f} qualitatively bears some resemblance of UCu_2Si_2, where a complex interplay of FM and a spin density wave (SDW) scenario gives rise to the observation of such kind of proximate phase transitions [66,67]. However, to conclusively elucidate this behavior in UBeGe, neutron diffraction measurements are required.

The temperature dependence of c_{5f} of UBeGe below $T_C^{(2)}$ deviates strongly from the sum of an electronic and a simple magnon contribution, which can be modeled by $c_{5f}/T = \gamma(0) + aT^2 \exp(-\Delta/T)$ [23]. The simulation of such a behavior is depicted in Fig. 8. Probably, such an ansatz is too simple to capture the complex magnetic ordering in UBeGe. Moreover, the description is also expected to fail when approaching T_C. The electronic $\gamma(0)$ is ≈13.0(1) mJ mol^{-1} K^{-2}, indicating a very weak mass enhancement of the conduction electrons in UBeGe.

The magnetic entropy S_{5f} for the $5f$ magnetism in UBeGe is obtained by integration of c_{5f}/T. The entropy (right scale in Fig. 8) attained just above the ordering temperature is 1.56 R, a value close to $R \ln 5$. As is usually the case for U-containing intermetallic compounds [68], this entropy is well below that of $R \ln 9$ or $R \ln 10$ expected for $5f^2$ (i.e., U^{+4}) or $5f^3$ (i.e., U^{+3}) configurations, which should be realized only when the classical LS coupling scheme is followed [3]. The entropy above $T_C^{(1)}$ still increases and it is difficult to derive the value at high T due to the limited accuracy of the $c_p(T)$ data.

F. Electronic structure

Relativistic spin-restricted LDA band-structure calculations were performed for UBeGe. Selected partial density of states (DOS) curves are shown in Fig. 9. The partially occupied $5f_{5/2}$ states form a narrow peak at the Fermi level [Fig. 9(b)]. The width of this peak (∼0.5 eV) is smaller than the width of the $5f_{5/2}$ states in, e.g., UPd_2Al_3 (∼0.7 eV) [69] or UO_2 (∼0.8 eV) [70], but comparable to the width of the U $5f_{5/2}$ peak in UPd_3 [71], supporting our conclusion that the U $5f$ states of UBeGe are rather localized. The DOS at E_F of 10.2 states eV^{-1} f.u.$^{-1}$ is significantly higher than the value estimated from the specific heat.

A comparison of the band structure of UBeGe with that of ThBeGe shows that U $5f$ states are located in a low-DOS

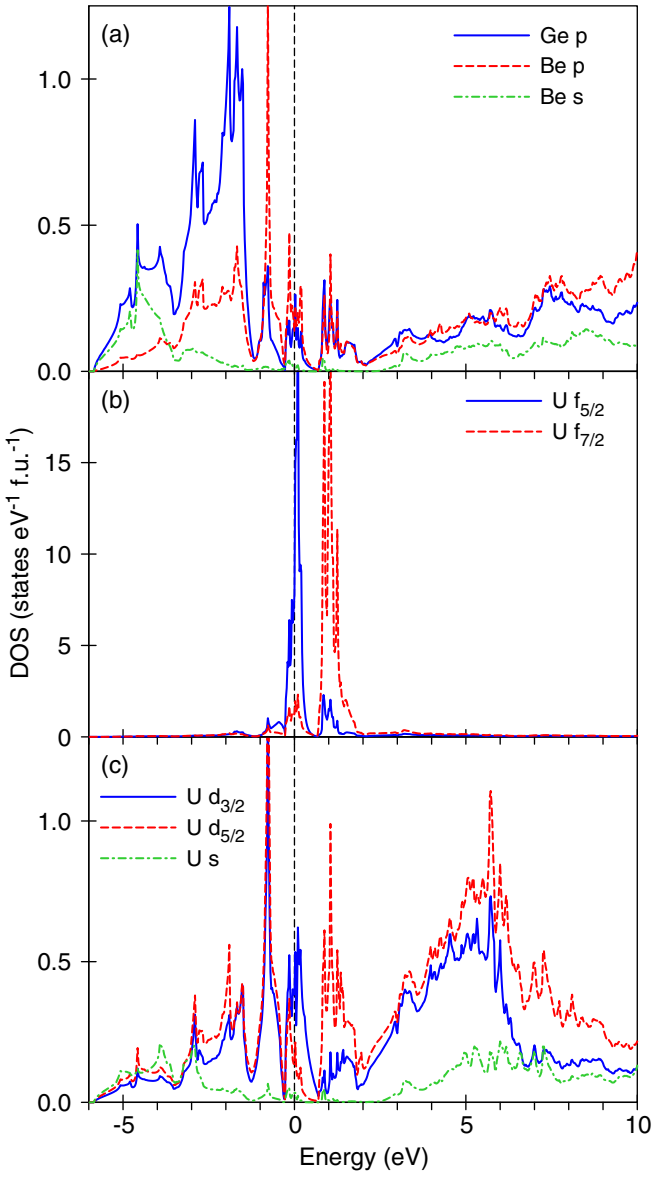

FIG. 9. Selected partial densities of states (DOS) obtained from relativistic spin-restricted calculations for UBeGe. For U $6d$ and $5f$ states densities of states with a total angular momentum $j = l \pm 1/2$ are shown.

region near the Fermi level which separates the occupied part of the valence band, formed predominantly by strongly hybridized Ge and Be p states, and unoccupied bands originating from U(Th) $6d$ states hybridized with the former. The low density of delocalized states at E_F and the weak hybridization of the corresponding bands with f states seems to be responsible for the localized character of the U $5f$ states in UBeGe. For ThBeGe, the DOS of 0.61 states eV^{-1} f.u.$^{-1}$ is in good agreement with the Sommerfeld coefficient.

The calculated f charge of 2.8 electrons inside the U atomic sphere deviates significantly from the f^2 state expected for a U^{4+} ion. However, one should keep in mind that the calculation for ThBeGe, with formally unoccupied Th $5f^0$ states, results in an f charge of 0.6 inside the Th atomic sphere, which is actually induced by a hybridization with delocalized states in a wide energy range. Subtracting the f charges for U and Th atomic spheres one obtains $f^{2.2}$ as a proper estimate for the occupation of localized U $5f$ states in UBeGe.

TABLE II. $5f$ charges inside the uranium atomic sphere and spin (μ_s), orbital (μ_l), and total ($\mu_l + \mu_l$) magnetic moments of uranium, calculated for the Coulomb repulsion U varying from 0 (LSDA) to 1.5 eV for UBeGe. The value of Hund's coupling $J = 0.5$ eV estimated from LSDA calculations was used. The calculations were performed assuming ferromagnetic order with the magnetization $\mathbf{M} \,||\, [010]$.

U (eV)	n	μ_s (μ_B)	μ_l (μ_B)	$\mu_s + \mu_l$ (μ_B)
0	2.80	1.84	−2.54	−0.69
0.5	2.84	1.77	−3.70	−1.93
1.0	2.82	1.81	−4.10	−2.30
1.5	2.79	1.82	−4.31	−2.49

Spin-polarized relativistic LSDA calculations performed assuming FM ordering of U moments confirm strong magnetocrystalline anisotropy in UBeGe. The lowest total energy is obtained when the U magnetization $\mathbf{M}$ is directed along [010], i.e., along the U–U bonds in the ab plane. The LSDA total energies calculated with $\mathbf{M} \parallel [1\bar{1}0]$ and $\mathbf{M} \parallel [001]$ are, respectively, 1.4 and 2.2 meV higher.

In this context, comparison with hexagonal U_3Ge_5 is interesting: There the orientation of the uranium magnetic moments (deduced from neutron diffraction) is due to two ferromagnetic components, one along the c axis and one within the ab plane [16].

Coming back to UGeBe, the energy of configurations with antiferromagnetic order along c is ≈40 meV higher. Accounting for spin polarization of U $5f$ states reduces $N(E_F)$ to 7.9 states eV^{-1} f.u.$^{-1}$ which is still higher than observed.

The calculated values of spin and orbital magnetic moments of U are $\mu_s = 1.87\,\mu_B$ and $\mu_l = -2.46\mu_B$ which gives the total U moment of $-0.59\,\mu_B$. This LSDA value is much smaller than the experimental saturation moment of $\approx 2.9\,\mu_B$, which is not surprising regarding the localized nature of the U $5f$ electrons in UBeGe.

However, the value of the U orbital moment strongly increases if electronic correlations in the U $5f$ shell are taken into account at the mean-field level using the rotationally invariant LDA+U approach [71,72]. The $5f$ charges inside the uranium atomic sphere and the U spin, orbital, and total moments obtained from LSDA and LSDA+U calculations with $\mathbf{M} \,||\, [010]$ are compared in Table II. As the U spin moment μ_s practically does not depend on U, the increase of the orbital moment μ_l brings the magnitude of the total uranium moment of 2.3–2.5 μ_B to better agreement with the high experimental value. Calculations for other magnetization directions reveal weak anisotropy of the orbital moment $\Delta\mu_l$, which increases with the increase of U from the LSDA value of $\Delta\mu_l = 0.1\,\mu_B$ to $\Delta\mu_l = 0.5\,\mu_B$ for $U = 1.5$ eV. The U $5f$ DOS from LSDA and LDA+U calculations are compared in Fig. 10. The Coulomb repulsion pushes two fully occupied $5f$ states to lower energy and strongly reduces the U $5f$ DOS at E_F which, nevertheless, remains finite due to small but finite occupation of the third U $5f$ state. It should be pointed out that the LDA+U approximation is too crude to properly describe the effect of electronic correlations in the uranium $5f$ shell.

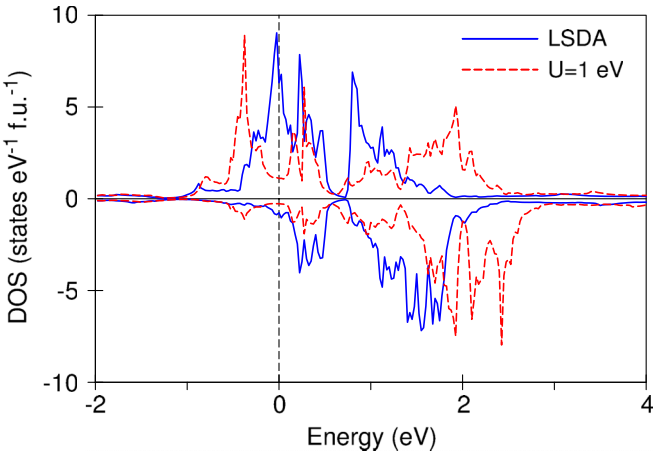

FIG. 10. Uranium $5f$ DOS of UBeGe from ferromagnetic LSDA and LDA+U ($U = 1$ eV) calculations.

IV. CONCLUSIONS

The new germanides UBeGe and ThBeGe crystallize with a ZrBeSi type of structure, which is closely related to the simple hexagonal AlB_2 prototype. The structural arrangement of UBeGe remains unchanged in the temperature range 100–300 K, and the U-U distances exceed the Hill limit, which hints toward a localized nature of U $5f$ states in the studied compound.

HERFD XANES at the UM_4 edge reveals the $5f^2$ configuration for the U atoms (i.e., oxidation state +4). A temperature dependence of the intensities of the XANES spectral features is observed for U-containing intermetallics for the first time. DFT simulations demonstrate that the changes are of magnetic origin, i.e., due to the FM ordering of the U moments.

The magnetization data indicate that UBeGe is a strongly anisotropic ferromagnet with $T_C = 157$ K, while ThBeGe is a diamagnet. The paramagnetic moment of UBeGe of 3.14 μ_B is similar to other systems with $5f^2$ configuration. For $T \ll T_C$, spectacular jumps occur in isothermal demagnetization curves of UBeGe. To clarify finally their origin, the influence of the magnetic anisotropy on the observed phenomena needs to be measured on high-quality single crystals.

The electrical resistivity of UBeGe shows Kondo-like behavior in temperature range 170–320 K and a double transition near the Curie point (161 and 153 K). The last observation suggests a complex magnetic ordering structure for UBeGe. A temperature-dependent neutron diffraction study will be required to get deeper insight into this problem. The strong anisotropy of the ferromagnetic state is reflected in the observed gap $\Delta = 10.7(3)$ K in the spin-wave excitation spectrum. The resistivity of ThBeGe is simply metallic.

Specific heat measurements on UBeGe reveal a clear magnetic anomaly with probably two transition at $T_C^{(1)} = 158$ K and $T_C^{(2)} = 150$ K, similar to the electrical resistivity. The magnetic entropy $S_{5f} \approx R \ln 5$ released at the ordering temperature is similar to that observed for other U-containing ferromagnets with $5f^2$ configuration. The specific heat data indicate that ThBeGe is a metal with low density of states at the Fermi level.

The electronic structure calculations confirm the $5f^2$ configuration for U in UBeGe as well as the metallic character of ThBeGe. The discrepancy between the experimentally observed saturation magnetization and the theoretically calculated total moment is explained by the strongly localized nature of the U $5f$ electrons.

ACKNOWLEDGMENTS

We thank L. Havela for his interest and helpful discussions. We also thank H. Borrmann for performing powder diffraction measurements, P. Merz for preparing and sealing the sample tube with powder and flammable liquid, and C. Geibel for fruitful discussions.

[1] G. Zwicknagl and P. Fulde, J. Phys.: Condens. Matter **15**, S1911 (2003).
[2] B. Coqblin, Acta Phys. Pol. A **121**, 1005 (2012).
[3] V. Sechovsky and L. Havela, in *Handbook of Magnetic Materials*, edited by K. Buschow (Elsevier, Amsterdam, 1998), Vol. 11, p. 289.
[4] J. Rieger, A. Mielke, E.-W. Scheidt, and G. Stewart, J. Alloys Compd. **221**, 42 (1995).
[5] R. Sobczak and P. Rogl, J. Solid State Chem. **27**, 343 (1979).
[6] R. Troć, M. Samsel-Czekała, E. Talik, R. Wawryk, Z. Gajek, and M. Pasturel, Phys. Rev. B **92**, 104427 (2015).
[7] W. Trzebiatowski, A. Śliwa, and B. Staliński, Roczniki Chemii **26**, 110 (1952).
[8] R. Troc and W. Suski, J. Alloys Compd. **219**, 1 (1995).
[9] V. Sechovsky and L. Havela, in *Ferromagnetic Materials*, edited by E. P. Wohlfarth and K. H. J. Buschow (Elsevier, Amsterdam, 1988), Vol. 4, pp. 309–491.
[10] L. Havela, M. Paukov, I. Tkach, Z. Matěj, D. Kriegner, S. Mašková, B. Vondráčková, M. Prachařová, I. Turek, M. Diviš *et al.*, J. Magn. Magn. Mater. **400**, 130 (2016).
[11] A. Alles, B. Falk, E. F. Westrum, F. Grønvold, and M. R. Zaki, J. Inorg. Nucl. Chem. **39**, 1993 (1977).
[12] P. Wiśniewski, A. Gukasov, and Z. Henkie, Phys. Rev. B **60**, 6242 (1999).
[13] T. Endstra, G. Nieuwenhuys, J. Mydosh, and K. Buschow, J. Magn. Magn. Mater. **89**, L273 (1990).
[14] A. Andreev, N. Mushnikov, F. Honda, V. Sechovský, P. Javorský, and T. Goto, J. Magn. Magn. Mater. **272–276**, E337 (2004).
[15] A. V. Andreev, M. Tomida, Y. Homma, Y. Shiokawa, V. Sechovský, N. V. Mushnikov, and T. Goto, J. Alloys Compd. **346**, 95 (2002).
[16] P. Boulet, M. Potel, G. André, P. Rogl, and H. Noél, J. Alloys Compd. **283**, 41 (1999).
[17] R. Troć, H. Noël, and P. Boulet, Philos. Mag. B **82**, 805 (2002).
[18] A. V. Kolomiets, J.-C. Griveau, J. Prchal, A. V. Andreev, and L. Havela, Phys. Rev. B **91**, 064405 (2015).
[19] A. Pikul, R. Troć, A. Czopnik, and H. Noël, J. Magn. Magn. Mater. **360**, 217 (2014).

[20] D. Aoki, A. Huxley, E. Ressouche, D. Braithwaite, J. Flouquet, J. P. Brison, E. Lhotel, and C. Paulsen, Nature (London) **413**, 613 (2001).

[21] K. Prokeš, Acta Phys. Pol. A **113**, 209 (2008).

[22] P. Manfrinetti, A. Palenzona, S. K. Dhar, and R. Kulkarni, J. Alloys Compd. **368**, 13 (2004).

[23] R. Troć, Z. Gajek, and A. Pikul, Phys. Rev. B **86**, 224403 (2012).

[24] S. S. Saxena, P. Agarwal, K. Ahilan, F. M. Grosche, R. K. W. Haselwimmer, M. J. Steiner, E. Pugh, I. R. Walker, S. R. Julian, P. Monthoux *et al.*, Nature (London) **406**, 587 (2000).

[25] V. P. Mineev, Phys.-Usp. **60**, 121 (2017).

[26] P. Boulet, A. Daoudi, M. Potel, H. Noél, G. Gross, G. André, and F. Bourée, J. Alloys Compd. **247**, 104 (1997).

[27] K. Machida and T. Ohmi, Phys. Rev. Lett. **86**, 850 (2001).

[28] D. P. Rojas, A. N. Medina, L. M. da Silva, and F. G. Gandra, J. Magn. Magn. Mater. **272–276(Suppl.)**, E11 (2004).

[29] D. P. Rojas, A. N. Medina, F. G. Gandra, and L. P. Cardoso, J. Appl. Phys. **93**, 7825 (2004).

[30] J. W. Nielsen and N. C. Baenziger, Acta Crystallogr. **7**, 132 (1954).

[31] A. Leithe-Jasper, H. Borrmann, and W. Hönle, Laboratory of High Safety Standard (LHS), Scientific report of Max-Planck-Institut für Chemische Physik fester Stoffe, Dresden, Germany (2006), p. 25.

[32] STOE Powder Diffraction Software, WINXPOW, ver. 2 (STOE and Cie GmbH, Darmstadt, Germany, 2001).

[33] L. Akselrud and Y. Grin, J. Appl. Crystallogr. **47**, 803 (2014).

[34] C. Gauthier, V. A. Solé, R. Signorato, J. Goulon, and E. Moguiline, J. Synchrotron Radiat. **6**, 164 (1999).

[35] P. Glatzel, T.-C. Weng, K. Kvashnina, J. Swarbrick, M. Sikora, E. Gallo, N. Smolentsev, and R. A. Mori, J. Electron Spectrosc. Relat. Phenom. **188**, 17 (2013).

[36] K. O. Kvashnina and A. C. Scheinost, J. Synchrotron Radiat. **23**, 836 (2016).

[37] O. K. Andersen, Phys. Rev. B **12**, 3060 (1975).

[38] V. Antonov, B. Harmon, and A. Yaresko, *Electronic Structure and Magneto-optical Properties of Solids* (Kluwer Academic, Dordrecht, Amsterdam, 2004).

[39] J. P. Perdew and Y. Wang, Phys. Rev. B **45**, 13244 (1992).

[40] P. Krypiakevych, *Structure Types of Intermetallic Compounds* (Nauka, Moscow, 1977).

[41] R.-D. Hoffmann and R. Pöttgen, Z. Kristallogr. **216**, 127 (2001).

[42] J. Emsley, *The Elements* (Clarendon Press, Oxford, 1998).

[43] H. Hill, in *Plutonium and Other Actinides*, edited by W. Miner (Metallurg. Soc. AIME, New York, 1970), p. 2.

[44] K. O. Kvashnina, S. M. Butorin, P. Martin, and P. Glatzel, Phys. Rev. Lett. **111**, 253002 (2013).

[45] R. Gumeniuk, K. O. Kvashnina, W. Schnelle, A. Leithe-Jasper, and Y. Grin, Phys. Rev. B **91**, 094110 (2015).

[46] K. O. Kvashnina, H. C. Walker, N. Magnani, G. H. Lander, and R. Caciuffo, Phys. Rev. B **95**, 245103 (2017).

[47] C. Booth, Y. Jiang, D. Wang, J. Mitchell, P. Tobash, E. Bauer, M. Wall, P. Allen, D. Sokaras, D. Nordlund, T.-C. Weng, M. Torrez, and J. Sarrao, PNAS **109**, 10205 (2012).

[48] G. Wortmann, Hyperfine Interact. **47**, 179 (1989).

[49] A. Menovsky, F. de Boer, P. Frings, and J. France, in *High Field Magnetism*, edited by M. Date (North-Holland, Amsterdam, 1983), p. 189.

[50] K. Prokeš, T. Tahara, T. Fujita, H. Goshima, T. Takabatake, M. Mihalik, A. A. Menovsky, S. Fukuda, and J. Sakurai, Phys. Rev. B **60**, 9532 (1999).

[51] R. Troć, J. Stępień-Damm, C. Sułkowski, and A. M. Strydom, Phys. Rev. B **69**, 094422 (2004).

[52] R. Troć, J. Magnetics (Korea) **9**, 89 (2004).

[53] T. Nishioka, G. Motoyama, S. Nakamura, H. Kadoya, and N. K. Sato, Phys. Rev. Lett. **88**, 237203 (2002).

[54] T. Nishioka, N. K. Sato, and G. Motoyama, Phys. Rev. Lett. **91**, 209702 (2003).

[55] T. Nishioka, G. Motoyama, and N. Sato, J. Magn. Magn. Mater. **272**, E151 (2004).

[56] E. Lhotel, C. Paulsen, and A. D. Huxley, Phys. Rev. Lett. **91**, 209701 (2003).

[57] Q. Li, X. Yuan, L. Xing, and M. Xu, Sci. Rep. **6**, 27712 (2016).

[58] W. Wernsdörfer, N. Aliaga-Alcalde, D. N. Hendrickson, and G. Christou, Nature (London) **416**, 406 (2002).

[59] Y. Otani, H. Miyajima, and S. Chikazumi, IEEE Trans. Magn. **25**, 3431 (1989).

[60] Y. Otani, J. M. D. Coey, B. Barbara, H. Miyajima, S. Chikazumi, and M. Uehara, J. Appl. Phys. **67**, 4619 (1990).

[61] A. Handstein, D. Eckert, K.-H. Müller, B. Wall, and W. Rodewald, IEEE Trans. Magn. **30**, 598 (1994).

[62] N. Mott and H. Jones, *The Theory of the Properties of Metals and Alloys* (Dover, New York, 1958).

[63] E. S. R. Gopal, *Specific Heat at Low Temperatures* (Plenum Press, New York, 1966).

[64] R. Troć, M. Samsel-Czekała, J. Stępień-Damm, and B. Coqblin, Phys. Rev. B **85**, 224434 (2012).

[65] M. S. Henriques, D. I. Gorbunov, A. V. Andreev, Z. Arnold, S. Surblé, S. Heathman, J.-C. Griveau, E. B. Lopes, J. Prchal, L. Havela, and A. P. Goncalves, Phys. Rev. B **89**, 054407 (2014).

[66] R. Troć, Z. Gajek, A. Pikul, H. Misiorek, E. Colineau, and F. Wastin, Phys. Rev. B **88**, 024416 (2013).

[67] F. Honda, N. Metoki, T. D. Matsuda, Y. Haga, and Y. Ōnuki, J. Phys.: Condens. Matter **18**, 479 (2006).

[68] S. Kawamata, H. Iwasaki, and N. Kobayashi, J. Magn. Magn. Mater. **104–107**, 55 (1992).

[69] A. N. Yaresko, V. N. Antonov, and B. N. Harmon, Phys. Rev. B **68**, 214426 (2003).

[70] M.-T. Suzuki, N. Magnani, and P. M. Oppeneer, Phys. Rev. B **88**, 195146 (2013).

[71] A. N. Yaresko, V. N. Antonov, and P. Fulde, Phys. Rev. B **67**, 155103 (2003).

[72] A. I. Liechtenstein, V. I. Anisimov, and J. Zaanen, Phys. Rev. B **52**, R5467 (1995).